Surfaces and Interfaces 94 (2026) 109563

Contents lists available at ScienceDirect

Surfaces and Interfaces

journal homepage: www.sciencedirect.com/journal/surfaces-and-interfaces

Chitosan-based composite coatings of upconverting $NaYF_4$: Yb, Tm nanoparticles and their energy transfer with Rhodamine 6G dye molecules

Balázs Borbás [a,b], Borbála Tegze [a,*], Emőke Albert [a], Dóra Hessz [a,c], Zsófia Keresztes [d], Miklós Kubinyi [a], János Madarász [e], Péter Márton [a], Norbert Nagy [f], Adél Sarolta Rácz [f], Péter János Szabó [b], Tamás Szabó [d], Zoltán Hórvölgyi [a,*]

[a] Department of Physical Chemistry and Materials Science, Faculty of Chemical Technology and Biotechnology, Budapest University of Technology and Economics, Műegyetem rkp. 3., H-1111 Budapest, Hungary
[b] Department of Materials Science and Engineering, Faculty of Mechanical Engineering, Budapest University of Technology and Economics, Műegyetem rkp. 3., H-1111 Budapest, Hungary
[c] MTA-BME Lendület Quantum Chemistry Research Group, H-1111 Budapest, Hungary
[d] Functional Interfaces Research Group, Institute of Materials and Environmental Chemistry, HUN-REN Research Centre for Natural Sciences, Magyar tudósok körútja 2., H-1117 Budapest, Hungary
[e] Department of Inorganic and Analytical Chemistry, Faculty of Chemical Technology and Biotechnology, Budapest University of Technology and Economics, Műegyetem rkp. 3., H-1111 Budapest, Hungary
[f] Institute for Technical Physics and Materials Science, HUN-REN Centre for Energy Research, Konkoly Thege Miklós út 29-33., H-1121 Budapest, Hungary

ARTICLE INFO

Keywords:
Upconversion
Nanoparticles
Coatings
Chitosan
Energy transfer
Dye molecules

ABSTRACT

Upconverting nanoparticles (UCNPs) emit visible and UV photons under near-infrared excitation, and can potentially be utilized in areas such as sensing, photodynamic cancer therapy or photovoltaic devices. In various applications, *e.g.* optical sensors, it is advantageous to immobilize UCNPs on a substrate using an embedding material. In this work, a novel composite coating design is presented, using chitosan biopolymer as a matrix to incorporate UCNPs, which is also shown to be a suitable coating system for studying energy transfer processes between UCNPs and organic molecules in aqueous media. $NaYF_4$: 20% Yb, 0.5% Tm UCNPs are prepared via solvothermal method and incorporated in chitosan biopolymer to prepare thin, transparent composite coatings on glass surfaces by a facile spin-coating process. It is observed that the presence of UCNPs provides a rough surface, and the surface of the particles protruding from the coating is covered by a thin chitosan layer. The emission intensity of the UCNPs remains high after immobilization in the chitosan layer, the expected upconversion emission peaks are observed in coating form. Energy transfer between UCNPs and Rhodamine 6G fluorescent dye molecules is confirmed to occur, both in UCNP aqueous suspensions and in the composite coatings. The chitosan layer can be permeated by aqueous solutions, enabling energy transfer between the embedded UCNPs within the coating and an organic species dissolved in aqueous medium. The UCNP@chitosan composite coating design presented in this work is suitable for various future applications, mainly thin film based sensors for detecting biomolecules or metal ions.

1. Introduction

Upconverting nanoparticles (UCNPs) are able to convert lower energy light, typically near infrared light, into higher energy, typically visible and ultraviolet light. This is made possible by the special properties of rare earth ions – the most often used dopants in UCNPs – which are able to absorb multiple photons in order to emit a photon of higher energy [1]. The UCNPs that were so far found to be the most efficient are built up of three major components: a low phonon energy host lattice (e.g. $NaYF_4$, LaF_3, CaF_2 [1,2]), doped with two different types of lanthanide ions, a so-called sensitizer and an activator ion. Sensitizer ions can efficiently absorb exciting radiation of a desired wavelength (e.g. Yb^{3+} ions are used for 980 nm excitation) and transfer their energy to a neighboring dopant ion, mainly the activator ions (e.g. Er^{3+}, Tm^{3+}, Ho^{3+}). Following multiple excitation steps, the activator ion relaxes via photon emission in the visible to ultraviolet range, depending on its

* Corresponding authors.
E-mail addresses: tegze.borbala@vbk.bme.hu (B. Tegze), horvolgyi.zoltan@vbk.bme.hu (Z. Hórvölgyi).

https://doi.org/10.1016/j.surfin.2026.109563
Received 26 November 2025; Received in revised form 9 April 2026; Accepted 11 May 2026
Available online 12 May 2026

energy levels.

UCNPs have a variety of promising applications, such as bioimaging, cancer therapy, solar cells, photocatalyst, optical sensors, anti-counterfeiting etc. [3–11] There are a number of fields in which development of coatings that contain UCNPs is an important research direction: for example, thin film systems used for sensing [12–15], solar cells [16,17], optoelectronic devices [18,19] and displays [20]. In the literature, there are examples of UCNPs coated onto various substrates from a suspension [18,21,22], without the use of any additives or materials to immobilize the particles on the surface. However, this approach is not suitable for the development of coating devices with stable structure and properties, that can be continuously used during a longer time period. For this reason, an important research direction is to embed UCNPs into a matrix material or immobilize the particles by depositing other layers on top of the UCNPs.

Torresan *et al* [23] deposited UCNPs onto a glass substrate via the spin-coating of ethanolic UCNP suspension, followed by an additional layer of mesoporous metal oxide (TiO_2, SiO_2, ZrO_2), with the long-term goal to develop temperature sensing optical devices. The composite coatings showed upconverting emission and were permeable due to the porous structure. Sivakumar *et al* [20] prepared composite coatings made of LaF_3: Yb, Tm particles embedded into a silica sol-gel coating, in order to develop thin films suitable for planar waveguides, flat panel displays and fiber amplifiers. Sudarsan *et al* [24] also used silica as matrix material to prepare composite coatings of UCNPs, and they found that incorporating the particles into the silica layer resulted in enhanced upconversion properties compared to simply doping the lanthanide ions into the silica matrix. The use of TiO_2 matrix material has also been researched, since TiO_2 is a relatively cheap semiconductor with good photoactivity and antibacterial property, and TiO_2 coatings of different structures can be easily prepared by the sol-gel method [25,26] in order to develop antibacterial surfaces, photocatalysts and solar cells among others. Thin films made of TiO_2 crystals doped with lanthanide ions were investigated for use in solar cells [27,28]. Coatings made of UCNP/TiO_2 core-shell nanoparticles [17] and dye-sensitized UCNPs embedded in a TiO_2 matrix [16] were also prepared for use in dye-sensitized solar cells.

Polymers are also often used as matrix materials: Lin *et al* [29] found poly(methyl methacrylate) (PMMA) to be a good matrix material to immobilize UCNPs on a glass substrate or even on heat-sensitive substrates, since an important advantage of using polymers over metal-oxides as a coating material is that no heat-treatment is needed after the deposition step. UCNPs were embedded into PMMA and deposited by spin-coating to prepare temperature sensors [30] and optoelectronic devices [19]. Polystyrene was used to incorporate UCNPs and pH sensitive dye molecules in order to develop CO_2 [12] and ammonia [13] optical sensors. Fluorocarbon resins [31] and poly(vinyl chloride) [14,15] were also investigated as matrix materials of UCNP composite coatings with the hope of developing solar cells and sensors. In these cases, dip-coating, solvent evaporation and knife-coating processes were utilized, respectively. Lyu *et al* [32] embedded UCNPs into P3HT and PMMA matrices by spin coating, showing that polymer polarity, viscosity, and solubility govern nanoparticle dispersion and achievable nanoparticle volume fraction in the coating.

Bio-based polymers as matrix materials are also desirable as environmentally friendly alternatives, for example Li *et al* [33] prepared cellulose nanocrystal based chiral photonic films which contained UCNPs, for use in 3D displays and optical storage devices; while Achatz *et al* [34] developed oxygen sensors based on UCNPs and oxygen probe molecules embedded in an ethyl-cellulose film. Wu *et al* [35] created UCNP containing polydopamine based biodegradable hydrogels, where the change in upconverting emission intensity could be used to monitor the degradation process. Chitosan biopolymer can also be a promising matrix material for thin coatings containing UCNPs, since it is an abundant and cheap bio-based material, mainly sourced from crustacean shells [36]; it is biocompatible and biodegradable; and it has good aqueous solubility in acidic solutions (up to pH 5). It can be used to make transparent, thin coatings on solid surfaces in a facile, environmentally-friendly process, without the need for organic solvents or heat treatment at elevated temperature. According to our previous research, the prepared chitosan layer is permeable to organic molecules *e.g.* dyes when immersed in an aqueous medium [37]. This may facilitate energy transfer processes between UCNPs and these organic molecules, which have great importance in applications of UCNPs. Chitosan was so far investigated only as a shell material for core-shell UCNPs developed for photodynamic therapy [38,39]; and in biocompatible nanocomposites (aerogels and microspheres) of UCNPs [40]. Duong *et al* found that chitosan also acts as a surface-stabilizing ligand, making $NaYF_4$: Yb, Er UCNPs dispersible in water; the resulting suspension can remain stable for several months [40].

This work presents a novel design of UCNP-containing composite coatings with chitosan biopolymer selected as matrix material to incorporate the UCNPs, since to the best of our knowledge, thin coatings of chitosan containing UCNPs were not yet investigated in the literature. The aim was to control the composition of the coatings and the deposition parameters in order to maximize the upconversion emission intensity. The interactions between the chitosan matrix and the UCNPs, and their role in the resulting coating structure and emission properties were investigated. The coatings with the most advantageous properties were also studied in dye–UCNP energy transfer measurements using model dye molecules. There are many applications, such as various optical sensor devices [12,13,15,41], dye-sensitized solar cells [16] and biomedicine [38,39,42], which are based on the energy transfer process between UCNPs and a fluorophore, such as a fluorescent organic dye, or a photosensitive molecule or nanomaterial (*e.g.* gold nanoparticles [41, 43]). Energy transfer processes in the case of UCNPs are fundamentally challenged by particle sizes larger than the distance required for efficient energy transfer, low activator (*i.e.* UCNP) quantum yields, complex energy migration, and quenching pathways. Carefully engineered core–shell architectures or thin and functional surface coatings are required for efficient Förster resonant energy transfer (FRET) [44]. UCNP-based FRET is highlighted as a crucial tool for the sensing of *e.g.* biomolecules or metal ions, deep-tissue bioimaging, and theranostics, where the unique NIR-excited, anti-Stokes emission of UCNPs enables low-background, highly sensitive readout of biomolecular interactions that are difficult to access with conventional fluorophores [45]. The medium that surrounds the UCNPs must enable the acceptor molecules to access the surface of the UCNPs for efficient FRET to take place. This is a crucial parameter in designing UCNP based devices for energy transfer based applications [44]. Moreover, many of these possible uses require the UCNPs to be immobilized on a substrate, hence the research of UCNP-containing composite coatings with high upconversion emission intensities is essential for future application.

2. Experimental section

Materials: All reagents were analytical grade and used without further purification. The following materials were used for the preparation of the samples: thulium(III) chloride hexahydrate (99.9%), ytterbium(III) chloride hexahydrate (99.9%), yttrium chloride hexahydrate (99.9%), sodium chloride (for analysis), ammonium fluoride (99.99%), poly(vinylpyrrolidone) (K-30, M_w = 40 000 Da), chitosan (medium molecular weight: 200 000–300 000 Da, degree of deacetylation: 75–85%, viscosity of 1 m/m% solution in 1 m/m% aqueous acetic acid: 563 cP), Rhodamine 6G dye (95%) were obtained from Merck (Darmstadt, Germany). Acetic acid (99.8%), 2-propanol (99+%) and ethanol (EtOH, 99.7+%) were obtained from Reanal (Budapest, Hungary). Purified distilled water (filtered with Adrona Integrity+ system to reach 18.2 MΩ cm) was used in the experiments.

Preparation of UCNPs: 0.5 mol% thulium and 20 mol% ytterbium-doped $NaYF_4$ nanoparticles were synthesized by solvothermal method using ethylene glycol as solvent and poly(vinylpyrrolidone) as

surfactant, based on a method originally reported by Lisjak *et al* [46]. The inorganic salts and PVP (weight ratio of $TmCl_3{\cdot}6H_2O$: $YCl_3{\cdot}6H_2O$: NH_4F: NaCl: $YbCl_3{\cdot}6H_2O$: PVP = 1: 40: 60: 60: 124: 366) were dissolved in ethylene glycol in Teflon beakers and then stirred at 80°C. The reaction mixture was transferred to a stainless steel autoclave (volume filled to 50%), and heat treated at 200°C for 12 h. The reaction equation can be seen in Eq. (1).

$$4\ NH_4F + 0.795\ YCl_3 + 0.200\ YbCl_3 + 0.005\ TmCl_3 + NaCl \rightarrow NaY_{0.795}Yb_{0.200}Tm_{0.005}F_4 + 4\ NH_4Cl \quad (1)$$

After cooling down to room temperature (RT), the product was washed with distilled water and ethanol by several centrifugation steps (HERMLE Z 36 HK, 2000 or 5000 rpm, 5 min). A schematic overview for the synthesis method can be seen in Fig. 1. The resulting stable ethanolic suspension was later used in characterization and the preparation of composite coatings. For preparation of aqueous UCNP-suspensions, the ethanolic suspension was centrifuged at 5000 rpm speed for 5 mins, the precipitate was then dispersed in purified distilled water via 5 min of vortex mixing (FALC) and 10 min ultrasonication (Simax, Elma, S 15 H Elmasonic).

Preparation of coatings: Composite coatings on glass substrates made of upconverting nanoparticles embedded in chitosan biopolymer matrix material were prepared by spin-coating method. The glass substrates were cleaned before the coating deposition via immersing for 1 min in detergent solution, then 10 m/m% sulfuric acid solution, followed by rinsing with 2-propanol and ethanol.

Some samples were also deposited on cleaned silicon wafers for the ellipsometry measurements. The chitosan solution was prepared by dissolving 0.5 g chitosan in 49.5 g of 1 m/m% acetic acid aqueous solution. The solution was stirred for 24 h, then centrifuged (4000 rpm for 30 min) to remove any insoluble (imperfectly deacetylated) chitosan particles. Appropriate amounts of UCNPs (centrifuged from ethanolic UCNP-suspension) were dispersed via 5 min of vortex mixing and 10 min ultrasonication in aqueous chitosan solution, resulting in a suspension with UCNP content of 5 or 10 mg mL^{-1}.

The coating deposition was carried out using Specialty Coating Systems 6800 Spin Coater device. 50 µL droplet of the chitosan solution or the chitosan and UCNP precursor suspension was placed in the middle of the substrate spinning at 7000 rpm speed, with dwell time of 60 s. 1 to 3 layers were deposited on the substrates, with 10 min RT drying steps between the layers. Reference coatings (UCNP/glass) without chitosan were also prepared, by deposition of a droplet of 10 mg mL^{-1} UCNP suspension in ethanol, using the same parameters during spin-coating as above. The coatings were then dried for 24 h at RT, in air. Fig. 2 shows the structure of the prepared coatings. A scheme of the coating process can be seen in Fig. S1.

Characterization of UCNPs: The morphology of the nanoparticles was characterized using a transmission electron microscope (JEOL JEM-100 CXII). Before the measurement, particles were spread onto a water–air interface, then transferred onto a Formvar film coated copper grid, to prepare a monolayer of the nanoparticles on the surface. Based on the TEM images, the average particle diameters and size distribution plots were determined by measuring at least 200 particles.

The crystallinity of the UCNPs was characterized by an X-ray diffractometer (Philips PANalytical X'pert Pro, Cu-Kα radiation, λ = 0,1542 nm). Powder samples were prepared from the ethanolic suspension of the particles by drying at 70°C. The measurement was carried out in the range of 2Θ = 4–84°, using scanning rate of 5 s/step and step size of 0.0167°. The average crystallite size was calculated from the four highest intensity peaks of the XRD pattern, using Scherrer's equation [47].

Zeta potential measurements (Malvern Zetasizer Nano ZS, Malvern Instruments Ltd., Worcestershire, UK) were carried out in DTS1070 disposable folded capillary cell over 2 hours at 25°C, at pH 7. Each data group consisted of the results of 5 consecutive measurements performed with a 5 s delay between each other, and a 20 s equilibration period before the first ones. Other measurement parameters were set to automatic and were performed as follows: attenuation was set to 9; the applied voltage was 150 V; 10–15 records were taken per measurement with an acquisition time of 3–5 s for each, general purpose analysis model was used. The sample in the capillary cell was sonicated in a water bath in an ultrasonicator (Elma Elmasonic S 30, Germany) for 2 min before the stability measurement.

Dynamic light scattering particle size evaluation was performed at 25°C with the same Malvern Zetasizer Nano ZS device as for the zeta potential measurements. The samples were filled in DTS0012 disposable plastic cuvettes. The measuring sequence was automated, using a fixed measuring position (6.5 mm) and attenuation (7). 30 measurements were carried out in 3 hours of monitoring. The duration of measurements was set to automatic; the data acquisition consisted of 10–15 records per measurement, lasting for 5–10 s each. 5 s equilibration time was added before every measurement and 120 s delay time after each one. Data analysis mode was set to general.

For instrument control, data collection and evaluation Zetasizer software (ver. 7.11) was used.

Characterization of the coatings: The surface morphology and roughness of the composite coatings were investigated by atomic force microscopy, using an AIST-NT SmartSPM 1000 AFM device in tapping mode with a PPP-NCHR20 NanoSensors needle (nominal radius of the needle < 20 nm). Height and phase images of the surfaces were recorded. The evaluation was performed using Gwyddion software. Scanning electron microscopy coupled with energy dispersive spectroscopy analysis (SEM-EDS) was carried out on an UCNP@chitosan coating sample (3-layered composite coating prepared from an aqueous 10 mg mL^{-1} UCNP-chitosan suspension), which was coated with a ~7 nm thick gold layer using a Bal-Tec SCD005 Sputter Coater, with 30 mA sputter current and 50 s sputtering time. The SEM images and EDS elemental maps were measured by a Hitachi TM4000Plus Tabletop Scanning Electron Microscope equipped with a BSE detector, with 20 kV accelerating voltage and 9.7 mm focal depth.

The wettability of the coatings was studied via water contact angle measurements (Krüss, DSA30) using the sessile droplet method. The

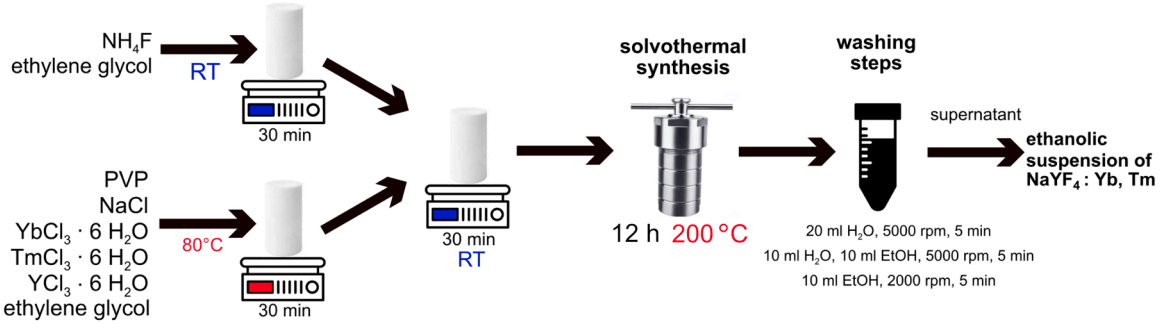

Fig. 1. Schematic illustration of the preparation steps of the nanoparticles (RT: room temperature).

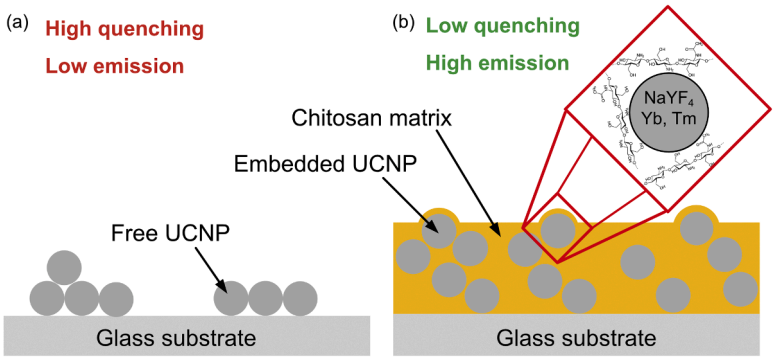

Fig. 2. Schematic illustration of the prepared coating systems: reference UCNP/glass samples (a) and UCNP@chitosan/glass composite coatings (b).

advancing and receding contact angles (purified distilled water–air–chitosan interface) of the reference chitosan coatings and UCNP-containing composite chitosan coatings were determined at RT and 70% humidity. The water contact angle was measured in real time from the digital image of the liquid drop using ADVANCE software (as seen in Fig. S2). For each measurement, the mean and standard deviation of the results were calculated from the data of 6 droplets.

XPS measurements were performed in a Thermo Scientific ESCALAB Xi+ instrument. The spectra were recorded applying Al Kα X-ray source (λ = 0.8340 nm, 1486.6 eV), the size of the X-ray spot was 900 μm. Depth profiling was performed by MAGCIS™ argon ion source operating in cluster mode (8 keV, cluster size 500, angle of incidence 45° respect to the surface normal) in an area with a diameter of 3 mm. Charge neutralizer was used in standard electrostatic mode. Survey spectra were measured in steps of 0.5 eV with 10 ms dwell time per data point. Carbon (1s), nitrogen (1s), oxygen (1s), fluorine (1s), sodium (1s), silicon (2p), and yttrium (3d) high-resolution spectra were measured within the spectral range of interest (ca. 20 eV around the core level emission peaks) at 30 eV pass energies with 0.1 eV steps and 50 ms dwell time per data point. Ytterbium and thulium were under the detection limit of the setup. After reducing the backgrounds, the atomic concentrations were obtained by applying the sensitivity factor library (Althermo1).

The transmittance spectra of the coatings were measured with a UV-Vis spectrophotometer (Analytik Jena Specord 200), in the wavelength range of 350–1100 nm, using air as reference, with 10 nm s^{-1} speed and 1 nm resolution. The thickness and effective refractive index (at 632.8 nm) values of the reference coatings (without UCNPs) were determined by the Hild-model [48,49].

Spectroscopic ellipsometry was used to characterize the thickness and refractive index of the chitosan coatings, using a Semilab's Sopra EP-12 ellipsometric porosimeter. Water vapor absorption was studied to characterize the hydrophilic properties of the bulk phase of the coatings. The absorption process leads to the swelling of the chitosan coatings, and hence to a change in effective refractive index and layer thickness values (thin chitosan coatings on glass substrates were proven to show constrained swelling in water, meaning that only the layer thickness increases without any lateral movement of the layer [50]). UCNP-containing and UCNP-free reference chitosan coatings on silicon substrates were investigated. Absorption and desorption (at decreasing water vapor) isotherms were recorded at 24°C in a vapor atmosphere of purified distilled water. Measurements were performed in the wavelength range 173.6–971.5 nm at a 60° (incidence) angle. Refractive index and initial film thickness at zero relative pressure were determined using the Cauchy model [51] with Semilab Ltd. SEA software.

Characterization of anti-Stokes emission and energy transfer processes: Upconversion emission was studied using a spectrofluorometer (Edinburgh Instruments Spectrofluorometer FS5) with a 980 nm monochromatic laser light source for excitation. The emission spectra of 1 mg mL^{-1} ethanolic suspensions of the UCNPs were measured in a quartz cuvette kept at 20.0°C, in the range of 300–700 nm, with a 1 nm step size, 0.5 s dwell time, 1.85 nm scan slit, and laser power of 1.49 W. Emission spectra of the model composite coatings were recorded with the same parameters, with the only difference being the use of a different sample holder suitable for solid samples, and adjusting the scan slit to 4.5 nm. In order to characterize the energy transfer process between UCNPs and fluorescence organic dye molecules, UCNPs were dispersed in aqueous Rhodamine 6G (R6G) dye solutions, and measured in a quartz cuvette, with the same parameters as above. The concentration of the dye varied from sample to sample (0–100 μM), while the UCNP content was kept constant (1 mg mL^{-1}). Similar measurements were carried out with the coating samples, by immersing the UCNP-containing chitosan matrix coating into dye solutions of varying concentrations (for more details see Fig. S3).

3. Results and discussion

3.1. Characterization of UCNPs

The XRD pattern of as-prepared $NaYF_4$: Yb, Tm particles is shown in Fig. 3. The crystal phase of the synthesized nanoparticles was cubic (α) $NaYF_4$ (PDF-04-019-2860), and the average crystallite size was estimated to be 24 ± 1 nm (see Supplementary Information for details).

The transmission electron microscopy image and the calculated size distribution of the nanoparticles are shown in Fig. 4. The particles had a close to spherical shape and a relatively narrow size distribution, with average particle diameter of (34 ± 7) nm. This is slightly higher compared to the estimated average crystallite size of 24 ± 1 nm based on

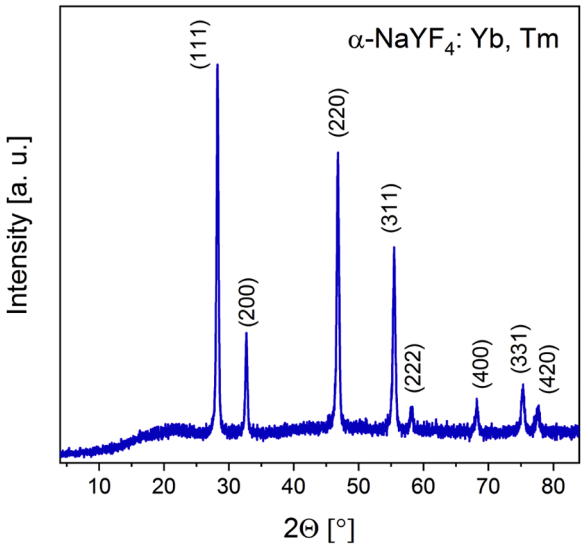

Fig. 3. X-Ray diffractogram of the $NaYF_4$: 20% Yb, 0.5% Tm UCNP powder sample.

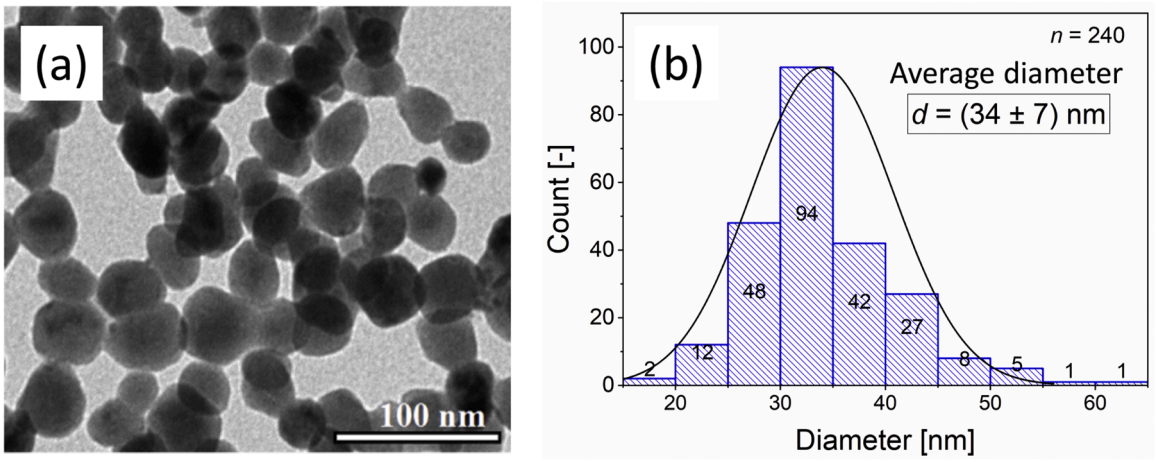

Fig. 4. TEM image (a) and size distribution (b) of $NaYF_4$: 20% Yb, 0.5% Tm UCNPs.

the XRD pattern. This difference is most likely due to the limitations of the Scherrer's equation in determining the particle size: strictly speaking, the equation determines the coherent diffraction domain size, not the crystallite size, which distinction can be important for multi-domain crystallites. Any crystal lattice strain and/or disorder contribute to the broadening of the measured peaks of the XRD pattern, which results in the underestimation of the coherent diffraction domain size [52]. Furthermore, the nanoparticles may have an ordered crystalline core surrounded by a shell, where the atoms near the surface form a more disordered, amorphous structure, which can also contribute to the underestimation of the particle size by XRD.

The zeta potential of UCNPs dispersed in water (1 mg mL^{-1}) was measured for 2.5 hours. As the results in Fig. S4 a show, the UCNPs have a positive surface charge, the measured values fall between +22 and +30 mV, with a minor (2.5 mV) increasing trend. In order to check long-term stability, an additional data point was measured after 6 hours, which also showed no significant change in zeta potential.

Dynamic light scattering (DLS) particle size measurements (see Fig. S4 b) showed that the hydrodynamic diameter of UCNPs in water was around 120 nm (with a polydispersity index of 0.136), suggesting that the nanoparticles are present in the aqueous phase as small aggregates. To investigate how aggregation affects other measurements carried out in water, a sedimentation study was conducted: sizes and count rate of scattered light were monitored for 3 hours.

It was found that within 2 hours the average particle diameter was ~122 nm, and in the 3rd hour it showed a slight increase to ~125 nm. The mean count rate also stayed constant for the first 2 hours, at around 305 kcps, while in the 3rd hour, similarly to the size, slightly increased as well. These results imply that within the practical application period the UCNPs do not suffer significant aggregation and/or sedimentation.

3.2. *Characterization of coatings*

The layer thickness of the coatings was characterized by UV-Vis spectroscopy and spectroscopic ellipsometry, the measured spectra were analyzed by thin film optical model fitting [49] to determine refractive index and layer thickness values (see Fig. S5 and Table S1 for detailed results).

According to the optical model fitting based on the transmittance spectra, the 3-layered reference chitosan coatings have an effective refractive index of $n_{eff} = 1.543 \pm 0.008$ and a layer thickness of $d = (162 \pm 5)$ nm. The transmittance spectra of the UCNP@chitosan/glass composite coatings showed light scattering due to the presence of the particles (see Fig. S5), and the thin film optical model could not be applied in this case, since the model assumes negligible light scattering. In order to investigate the layer thickness of the composite coatings, and to study their behavior in aqueous medium, spectroscopic ellipsometry measurements were carried out by applying such an optical model which can also consider the light scattering of the coating. The spectroscopic ellipsometric characterization (see Fig. S6) of the chitosan and UCNP@chitosan coatings formed on Si substrate showed that the layer thickness of the UCNP-free reference chitosan coating was 95 nm (the difference from the 162 nm value determined by UV-Vis spectroscopy is most likely due to the different substrate used in this measurement), while that of the UCNP-containing composite chitosan coatings was 109 nm. As the relative pressure of water vapor increased during the measurement, the thickness of the coatings increased to 131 nm and 135 nm, respectively, due to water uptake, since the chitosan coating can swell by absorbing water. The results indicate that the prepared chitosan-based composite coatings are permeable by water molecules, which is a useful property for energy transfer based applications.

SEM-EDS analysis (Fig. 5 and Fig. S7) confirmed the presence of Na, Y, F, and Yb in the UCNP@chitosan coating, while Tm (0.5 mol%) remained below the detection limit. It can be seen in Fig. 5. that the F and Y elemental maps (providing information only from the top layer of the coating due to lower photon energy of Y Lα1 (~1.9 keV) and F Kα1,2 (~0.68 keV) emission lines) clearly show the position of the nanoparticles on the sample surface, in accordance with the SEM image: the $NaYF_4$:Yb,Tm nanoparticles are present throughout the entire investigated area, but their larger aggregates, in which particles are present in a higher amount on the surface, are clearly visible as brighter spots. In contrast, Na and Yb exhibit a homogeneous distribution (Fig. S7). The uniform Na signal most likely originates from the soda-lime-silica glass substrate. The emission line of Yb Lα1 has a higher ~7.4 keV photon energy, thus the Yb elemental map also includes information from the deeper parts of the coating. This implies that UCNPs are present not just on the surface, but are homogeneously incorporated throughout the entire thickness of the chitosan layer.

The atomic force microscopy (AFM) images of UCNP-containing composite chitosan coatings on a glass substrate are shown in Fig. 6.

The distribution of nanoparticles in the coating is not uniform: the particles are aggregated in 'islands' of ~400 nm, which in many cases protrude from the chitosan layer, resulting in a rough surface (Fig. 6a). The surface roughness factor (the ratio of the real surface area to the geometric 'surface view' area) of the composite coatings was determined to be $f = 1.078$, while the surface of UCNP-free chitosan coatings is smooth ($f \cong 1$) [53]. The presence of aggregates in the coating is not surprising, since the previously described DLS results also showed aggregation in aqueous media. It is important to investigate whether the particles protruding from the surface are covered by a thin layer of chitosan, or if the parts of the particles that are raised above the surface of the chitosan layer are completely bare, since the surface properties of

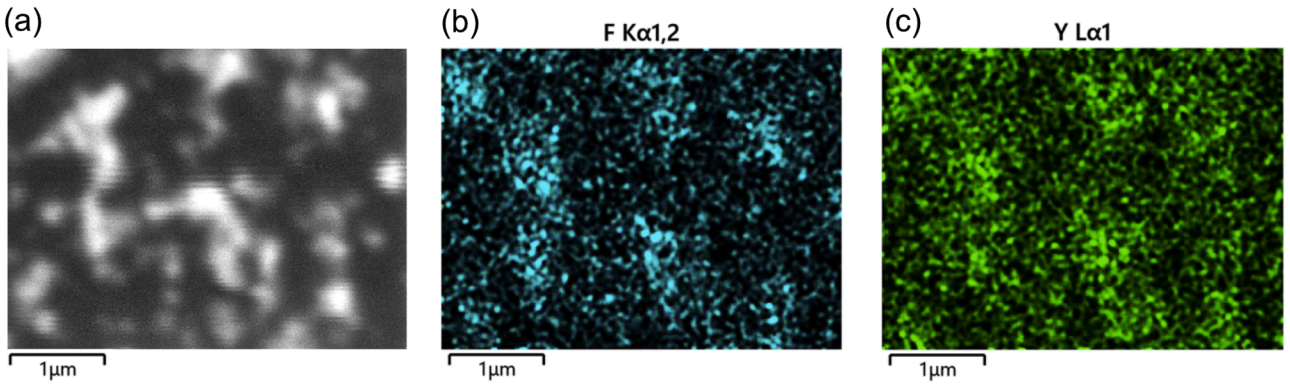

Fig. 5. SEM image (a), and corresponding EDS elemental maps of F (b) and Y (c) measured on UCNP@chitosan coating sample (3-layered composite coating prepared from an aqueous 10 mg mL^{-1} UCNP-chitosan suspension) coated with a gold layer.

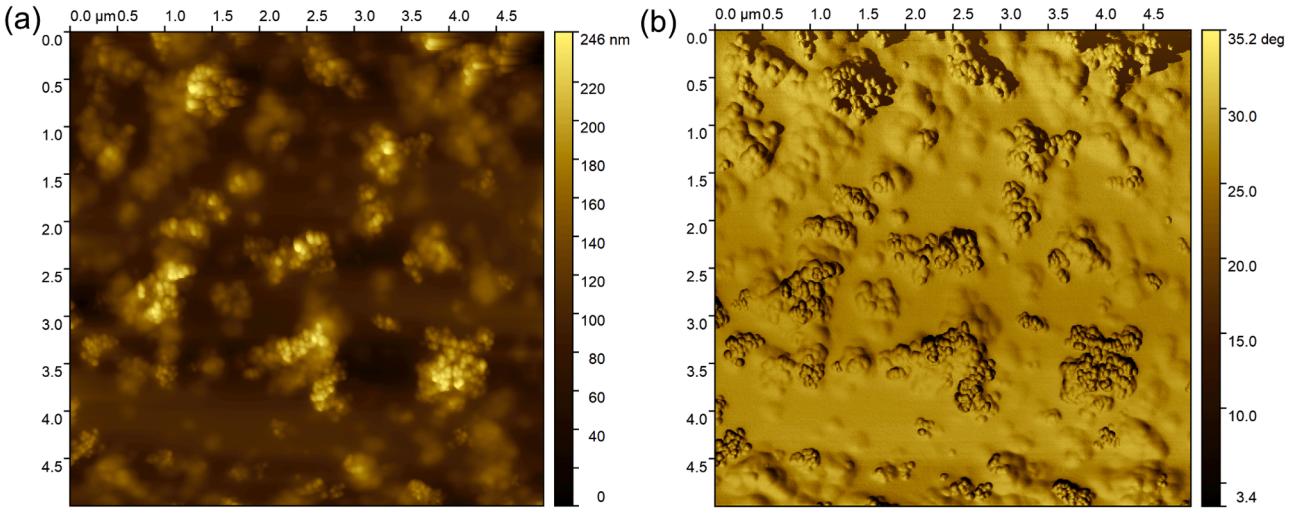

Fig. 6. (a) Height image (*i.e.* the measured height in the sampled area in nanometers) and (b) phase image (*i.e.* the measured phase angle in the sampled area in degrees) of UCNP@chitosan coatings recorded with AFM (on a 3-layered composite coating prepared from an aqueous 10 mg mL^{-1} UCNP-chitosan suspension).

the particles can significantly influence the upconversion emission properties [54]. According to the phase image obtained from the AFM measurements (Fig. 6b), it can be observed that while the variation of ca. 30° within the image is considerable, it can be observed only along the sides of the protruding features and, more prominently, in the regions between them, where the surface–tip interaction is stronger due to geometrical reasons. Therefore, the phase image essentially reflects the topography. On top of the protruding UCNPs the phase characteristic of the flat chitosan surface is consistently observed (that is, the top of all particles appears bright in the image), which indicates that the UCNPs are coated with chitosan.

To further investigate this question water contact angle measurements and X-ray photoelectron spectroscopy (XPS) combined with argon gas cluster sputtering were carried out. The measured water contact angles are shown in Table 1.

Slightly lower water contact angles were measured on the composite coatings, compared to the UCNP-free reference chitosan coatings. Based on the AFM images, the composite coatings have a rough surface, and consequently the measured contact angle values are so-called apparent contact angles. If the roughness factor of the surface is not very high, it can be assumed that the water shows homogeneous wetting on the surface: the water displaces all air from the surface irregularities and maintains direct contact with the surface of the coating (Wenzel's homogeneous wetting model [55]). Based on the roughness factor determined by AFM and the Young's contact angles measured on the smooth surface of the reference chitosan coatings, the apparent contact angle of a chitosan coating with a rough surface can be calculated, assuming that the entire surface is chemically uniform, *i.e.* the upconverting particles are covered by a thin layer of chitosan (see details in Supplementary Information). This calculated value was found to be (36 ± 4)°, which should be equal to the (32 ± 2)° value measured on the composite coatings, if the particles are truly covered by chitosan. Our calculation is within the error range, indicating that the decrease in the water contact angle can be explained by the roughness of the surface alone, suggesting that the UCNP-aggregates protruding from the coating surface are covered with a thin layer of chitosan.

A more rigorous analysis of the interfacial layer composition was carried out via XPS depth profiling. The results show the atomic composition of the reference chitosan coating and the UCNP@chitosan/glass coating as a function of argon gas cluster sputtering time (Fig. 7, see details in Supplementary Information, Table S2). The sputtering time

Table 1
Water contact angles measured on reference chitosan/glass and composite UCNP@chitosan/glass surfaces.

	chitosan/glass	UCNP@chitosan/glass
Advancing contact angle (θ_A)	(53 ± 4)°	(41 ± 5)°
Receding contact angle (θ_R)	(27 ± 3)°	(21 ± 2)°
Contact angle hysteresis (θ_H)	(25 ± 2)°	(20 ± 2)°
Young's contact angle (θ_Y)	(42 ± 3)°	(32 ± 2)°

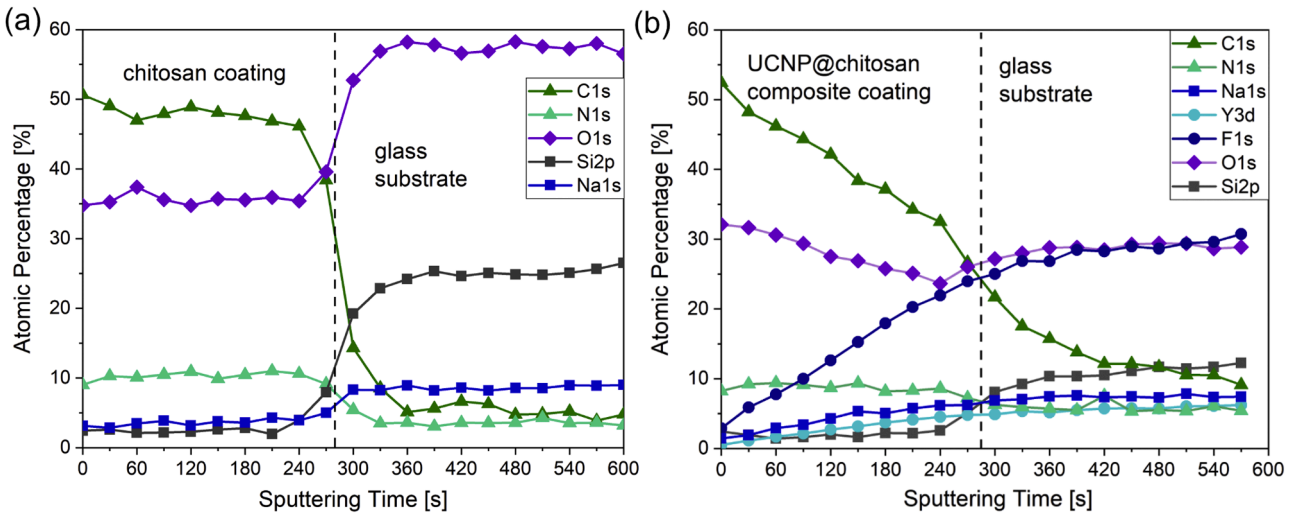

Fig. 7. Atomic composition of (a) reference chitosan/glass samples and (b) UCNP@chitosan/glass composite coatings as a function of sputtering time according to the XPS depth profiling results (of 3-layered coatings deposited from a 10 mg mL^{-1} precursor).

at which the glass substrate was reached is shown on the images, which was identified based on the increase of the Si peak signal. In the case of the reference chitosan coating, the atomic percentages of chitosan constituents (C, N) decrease sharply at the thin film/substrate interface. In the case of the UCNP-containing composite coating, the percentages of chitosan constituents are high at the top of the thin film, and they gradually decrease in the deeper layers of the coating, while the signals of UCNP constituents (mainly Y and F) gradually increase (the signals of Yb and Tm dopant ions are below the detection limit). This result indicates that there is chitosan present at the topmost layer of the coating, suggesting that the UCNPs protruding from the surface are not bare; they are covered by a thin chitosan layer. Interestingly, the signals of Y and F still show a slow increase after the glass substrate is theoretically reached, based on the C and N signals. The amount of Y increases from 0.5 at% to 6.2 at%, while the amount of F increases from 2.9 at% to 30.7 at%, a roughly 10 times increase in both cases (Table S2). This result suggests that the upconverting nanoparticles could not be completely removed from the surface by argon gas cluster sputtering, and/or these inorganic materials could adhere to the surface as contaminants after sputtering.

In brief, both water contact angle and XPS measurements show that the UCNP aggregates on the surface of the thin film are covered with chitosan and do not come into direct contact with the external environment.

3.3. Upconversion emission properties and energy transfer with model dye molecules

3.3.1. Upconverting emission of UCNPs in aqueous suspension and in coatings

The upconversion emission spectrum with the corresponding energy level transitions of aqueous 1 mg mL^{-1} $NaYF_4$: Yb, Tm upconverting nanoparticle suspension is shown in Fig. 8a. The energy level transitions agree with those reported in the literature [56].

Upconversion emission intensities of reference UCNP/glass coatings and UCNP@chitosan/glass composite coatings are compared in Fig. 8b. The emission spectra of chitosan matrix composite coatings prepared with different deposition parameters were also compared (see Fig. S8): emission intensity increased with increasing layer thickness and precursor UCNP-content, and the samples with 3 layers and an initial 10 mg mL^{-1} UCNP-concentration in the precursor suspension showed the highest emission intensities. Based on the results it can be concluded that immobilizing the UCNPs in chitosan matrix was needed to achieve high upconversion emission intensity (see Fig. 2). This can be explained by the higher amount of nanoparticles that can be fixed on the substrate by incorporation in a chitosan layer, if optimal deposition parameters

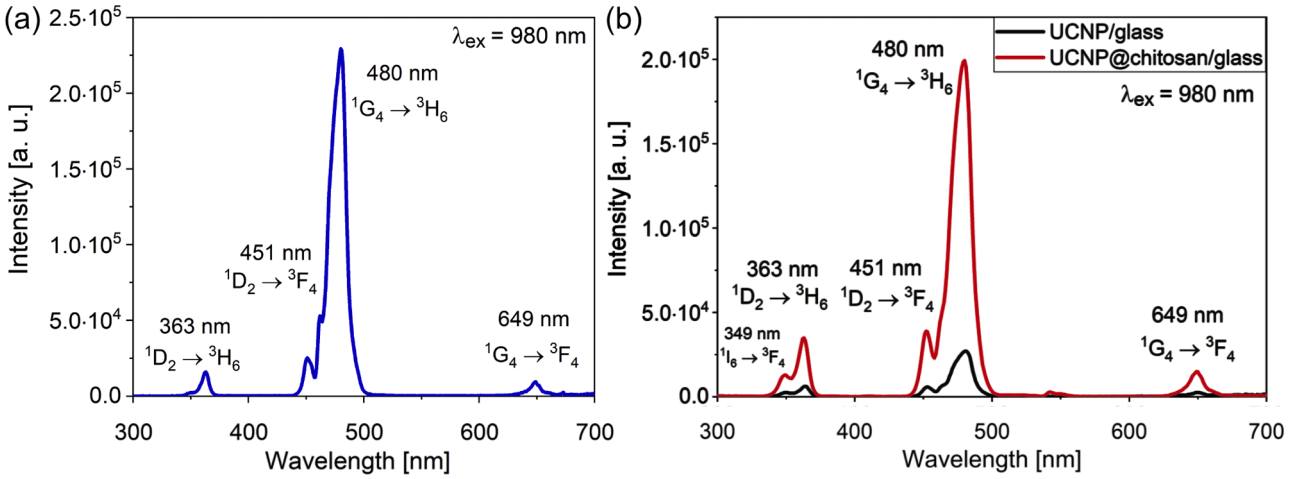

Fig. 8. (a) Emission spectrum of 1 mg mL^{-1} aqueous $NaYF_4$: 20% Yb, 0.5% Tm UCNP suspension, (b) Emission spectra of 3-layered coatings prepared from 10 mg mL^{-1} ethanolic UCNP suspensions and UCNP–chitosan suspensions.

are chosen. Using a viscous chitosan-based suspension as precursor during the spin-coating process can result in a thicker coating and better nanoparticle distribution on the surface, which is underlined by the similar results of Lyu *et al* [32]. Furthermore, the chitosan biopolymer covering the surface, and creating a thin inert shell around the nanoparticles, may perform a protective function similar to that of organic surface ligands which are added during various UCNP synthesis processes [54].

3.3.2. *Study of energy transfer process with Rhodamine 6G dye molecule*

The energy transfer interactions between upconverting nanoparticles and organic molecules are of utmost importance in many applications (*e.g.* drug-release systems, photovoltaic devices, optical sensors). Energy transfer studies were carried out using Rhodamine 6G (R6G) fluorescent dye as a model material. Energy transfer between the prepared UCNPs and the dye molecules can be achieved due to the emission of the $NaYF_4$: Yb, Tm particles in the 440–500 nm wavelength range partially overlapping with the absorption peak of R6G (see Fig. S9). Preliminary experiments were performed in order to evaluate the stability of the UCNP@chitosan coatings in water and in aqueous R6G solution (see details in Supplementary Information Fig. S10.) It was found that the emission intensity of the composite coatings remains unchanged over a 4 h time period in aqueous environments. This result is a promising sign for the possibility of using these composite coatings in future applications where the thin film system operates in an aqueous medium, or in an outdoor environment where humidity and rain are a concern. Although it goes beyond the scope of our present paper, it should be noted that in future research the long-term stability of the coating system must be evaluated, as degradation of the chitosan may occur after longer periods of time.

Fig. 9 shows the emission spectra of aqueous suspensions of 1 mg mL^{-1} $NaYF_4$: Yb, Tm particles and 1–20 μM R6G dye. It can be seen that if there are no dyes in the system, the UCNPs emit photons both in the visible and UV region of electromagnetic radiation as a result of the 980 nm excitation, but no emission peak can be detected at 554 nm wavelength, which is the characteristic wavelength of the R6G dye fluorescent emission. In preliminary experiments it was also confirmed that when the R6G dye solution (without UCNPs present) is subjected to 980 nm excitation, no emission is observed at all, since the dye is non-absorbent at this NIR wavelength (its absorption maximum is at 530 nm). However, if both UCNPs and R6G dyes were present in the suspension, it was observed that with increasing dye concentration the intensity of the 480 nm emission peak continually decreased, while a new emission peak appeared at 554 nm which showed continually increasing intensity. This result indicates that an energy transfer process could occur between the UCNPs and the R6G molecules in this system: the UCNPs were excited by 980 nm irradiation and emitted light around 480 nm, which could be absorbed by the R6G molecules, which in turn were able to emit light at 554 nm.

It is important to investigate whether this energy transfer process can also take place if the UCNPs are immobilized in a chitosan matrix and used in composite coating form. The emission spectra of UCNP@chitosan/glass composite coating samples (3-layered, prepared from a 10 mg mL^{-1} UCNP–chitosan suspension) immersed in aqueous R6G dye solutions of different concentrations can be seen in Fig. 10. Similarly to the previous results, under 980 nm excitation the emission peak characteristic of the R6G dye was detected, indicating that energy transfer occurred. The mechanism of the energy transfer process between UCNPs and R6G dye molecules is most likely Förster resonant energy transfer (FRET), as reported previously in case of suspensions [57]. FRET requires small distances between the donor and acceptor (a Förster distance of < 10 nm is reported in most cases of energy transfer between fluorophores and UCNPs [44]), which in the case of the composite coatings necessitates that the dyes are able to penetrate the chitosan matrix material and reach the surface of the UCNPs.

In our previous research [37], it was found that when thin chitosan coatings on glass substrates are immersed in an aqueous solution, the chitosan is able to swell, and the resulting thin hydrogel coating is permeable to small molecules, such as R6G dye molecules. Thus, it can be assumed that when the UCNP@chitosan composite coatings are immersed in the R6G aqueous solutions, the distance between the dye molecules and UCNPs is not significantly increased compared to the dye-containing UCNP suspensions, since the chitosan layer is permeable and the dye molecules diffusing into the chitosan hydrogel matrix can interact with the UCNPs.

It can be seen in Fig. 10b that with increasing dye concentration the intensity of the observed emission bands reached saturation, as opposed to the results in suspensions, which showed continuous increase or decrease in intensity (Fig. 9b). This suggests that energy transfer occurs through short-range interactions and that there is a maximum amount of dye in the composite coating that can interact with UCNPs embedded in the chitosan matrix material. It can be assumed that at the higher dye concentrations (*i.e.* above 20 μM, which is atypical for conventional fluorescence studies, but suitable for efficient energy transfer) the limited surface of the embedded UCNPs becomes saturated with R6G molecules, thus further increasing the bulk dye concentration results in no significant change in the fluorescence emission intensity of the dye molecules. This strengthens the statement that the phenomenon can be

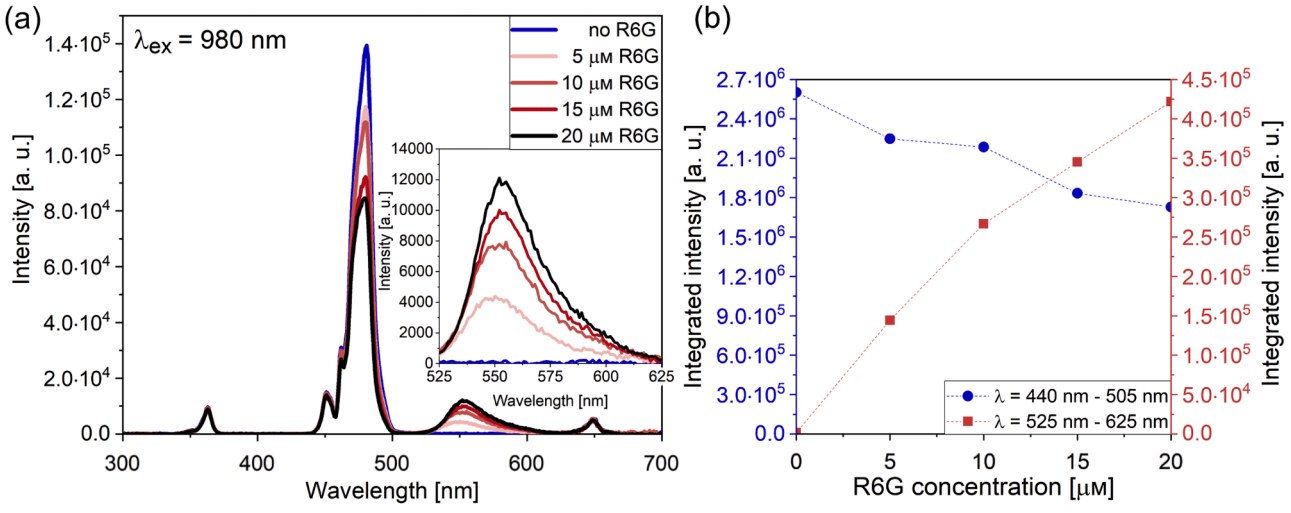

Fig. 9. (a) Emission spectra (inset: fluorescence band of R6G dye) and (b) intensity values integrated between 440–505 nm (UCNP emission peak) and 525–625 nm (R6G fluorescence emission peak) of 1 mg mL^{-1} aqueous UCNP suspensions with a R6G dye concentration of 0–20 μM.

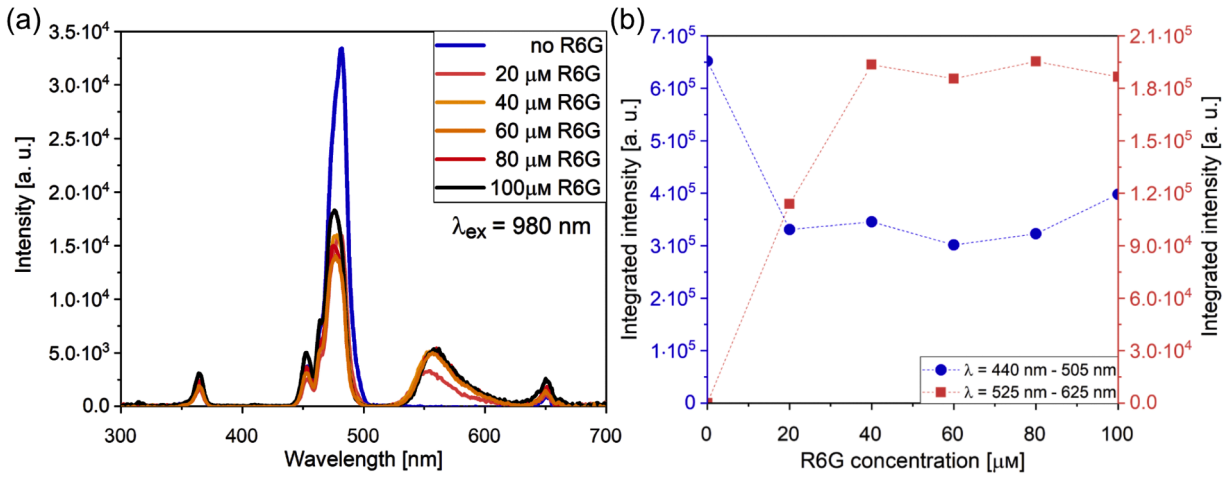

Fig. 10. (a) Emission spectra and (b) intensity values integrated between 440–505 nm (UCNP emission band) and 525–625 nm (R6G fluorescence emission band) of chitosan matrix composite coating (3-layered, prepared from a 10 mg mL^{-1} UCNP-chitosan suspension) immersed in an aqueous R6G dye solution of 0–100 μM concentration.

explained using FRET mechanism, however, further studies are required to determine the exact mechanism of the energy transfer process between dye molecules and UCNPs embedded in composite coatings.

It is also important to note, that the observed changes might be partially due to the higher dye concentrations that were necessary to study the energy transfer process in the coating samples, in comparison to the lower concentrations used when investigating UCNPs in suspensions. According to the literature [58], at concentrations above 20 μM the fluorescence quenching due to the dimerization of R6G molecules becomes noticeable. However, if the observed intensity change of the fluorescence band was solely caused by this quenching effect, then one could expect that the 480 nm emission band of the UCNPs would still continue to decrease with increasing dye concentration for the entire concentration range. It can be observed in Fig. 10 that this is not the case, suggesting that while fluorescence quenching at high concentrations might be a contributing factor, it cannot be the only reason for the observed changes.

The results show that chitosan matrix material is suitable for the preparation of composite coatings containing UCNPs, which can be used in applications requiring energy transfer with organic dye molecules in an aqueous phase (*e.g.* optical sensors).

4. Conclusion

$NaYF_4$: 20% Yb, 0.5% Tm upconverting nanoparticles (UCNPs) with cubic (α) crystal structure and an average diameter of 34 nm were synthesized via solvothermal method. As a novel approach in preparing UCNP-based nanocomposite materials, thin coatings of upconverting nanoparticles embedded in chitosan biopolymer matrix material were prepared on glass substrates by a facile spin-coating process. The UCNPs showed the expected anti-Stokes emission peaks under 980 nm NIR-excitation both in their aqueous suspensions and in coating form. According to the results, chitosan – a naturally sourced, renewable, biocompatible, and biodegradable biopolymer – has several advantages as a matrix to immobilize the UCNPs on a solid substrate: a high amount of UCNPs could be incorporated into the coating using a simple, one-step deposition from a non-toxic, aqueous suspension followed by drying at room temperature, without the need of post-treatments (*e.g.* annealing at high temperature). The composite chitosan coatings showed significantly higher emission intensities compared to the much less effective method of coating UCNPs onto glass by spin-coating from an ethanolic suspension. The results of AFM, XPS and water contact angle measurements confirmed that a thin layer of chitosan covers the UCNPs protruding from the surface of the composite coating: this chitosan layer covering the surface of the UCNPs may also have a protective function similar to organic surface ligands, leading to enhanced upconversion emission intensity. Moreover, due to the water-permeable nature of chitosan, the composite coatings are suitable for applications that require an energy transfer process between the UCNPs in the coating and an organic molecule in a liquid system: the chitosan layer is able to show swelling in aqueous medium, which enables the diffusion of the organic molecules into the composite coating.

The energy transfer process between upconverting nanoparticles and Rhodamine 6G model fluorescent dye molecules was investigated in suspensions of UCNPs dispersed in aqueous dye solutions, and also by immersing UCNP-containing composite chitosan coatings in aqueous dye solutions. In all cases, the fluorescence peak of R6G appeared under NIR (980 nm) excitation if UCNPs were present in the system, confirming that the upconverting nanoparticles can excite the dye molecules under NIR irradiation. It was proven that the energy transfer between UCNPs and the model dye molecules is possible even when UCNPs are incorporated into the chitosan film.

According to the results, these composite thin coatings of UCNPs, using chitosan biopolymer as a novel matrix material, are promising for a variety of applications in which UCNPs need to be immobilized on a solid substrate (*e.g.* thin film based optical sensors for the detection of biomolecules and/or metal ions), and also as model systems for studying energy transfer processes with organic molecules, which – due to the biomimicking structure and composition of chitosan biopolymer – can be beneficial in modelling the possible biomedical applications of UCNPs.

CRediT authorship contribution statement

Balázs Borbás: Writing – original draft, Visualization, Investigation. **Borbála Tegze:** Writing – original draft, Investigation, Conceptualization. **Emőke Albert:** Investigation, Formal analysis. **Dóra Hessz:** Investigation, Formal analysis. **Zsófia Keresztes:** Investigation, Formal analysis. **Miklós Kubinyi:** Writing – review & editing, Formal analysis. **János Madarász:** Investigation, Formal analysis. **Péter Márton:** Writing – review & editing, Formal analysis. **Norbert Nagy:** Investigation, Formal analysis. **Adél Sarolta Rácz:** Investigation, Formal analysis. **Péter János Szabó:** Supervision, Formal analysis. **Tamás Szabó:** Investigation, Formal analysis. **Zoltán Hórvölgyi:** Writing – review & editing, Supervision, Funding acquisition, Conceptualization.

Declaration of competing interest

The authors declare that they have no known competing financial interests or personal relationships that could have appeared to influence the work reported in this paper.

Acknowledgements

The authors thank András Szilágyi, Attila L. Kovács, Darja Lisjak, Róbert Kovács and Máté Burovincz for their contributions to this research work. This work was supported by the EKÖP-24-2-BME-348, EKÖP-25-3-BME-146 and STARTING 152904 Programs of the Ministry for Culture and Innovation of Hungary from the National Research, Development and Innovation Fund. This research is part of projects no. TKP2021-NVA-02 and TKP2021-EGA-02, which have been implemented with the support provided by the Ministry of Culture and Innovation of Hungary from the National Research, Development and Innovation Fund, financed under the TKP2021-NVA and TKP2021-EGA funding scheme. The Semilab's Sopra EP-12 ellipsometric porosimeter used for this research work is in possession of *Semilab Ltd.*

Supplementary materials

Supplementary material associated with this article can be found, in the online version, at doi:10.1016/j.surfin.2026.109563.

Data availability

Data will be made available on request.

References

[1] M. Haase, H. Schäfer, Upconverting nanoparticles, Angew. Chemie - Int. Ed. 50 (2011) 5808–5829, https://doi.org/10.1002/anie.201005159.
[2] L.G. Jacobsohn, C.J. Kucera, T.L. James, K.B. Sprinkle, J.R. DiMaio, B. Kokuoz, B. Yazgan-Kukouz, T.A. DeVol, J. Ballato, Preparation and characterization of rare earth doped fluoride nanoparticles, Materials 3 (2010) 2053–2068, https://doi.org/10.3390/ma3032053.
[3] C. Altavilla, Upconverting Nanomaterials Perspectives, Synthesis, and Applications, CRC Press Taylor & Francis Group, Boca Raton, 2016, https://doi.org/10.1201/9781315371535-5.
[4] A. Bagheri, H. Arandiyan, C. Boyer, M. Lim, Lanthanide-doped upconversion nanoparticles: emerging intelligent light-activated drug delivery systems, Adv. Sci. 3 (2016) 1–25, https://doi.org/10.1002/advs.201500437.
[5] G. Liang, H. Wang, H. Shi, H. Wang, M. Zhu, A. Jing, J. Li, G. Li, Recent progress in the development of upconversion nanomaterials in bioimaging and disease treatment, J. Nanobiotechnol. 18 (2020) 1–22, https://doi.org/10.1186/s12951-020-00713-3.
[6] T. Liang, J. Fu, M. Li, H. Li, Y. Hao, W. Ma, Application of upconversion photoluminescent materials in perovskite solar cells: opportunities and challenges, Mater. Today Energy. 21 (2021), https://doi.org/10.1016/j.mtener.2021.100740.
[7] N. Dubey, S. Chandra, Upconversion nanoparticles: recent strategies and mechanism based applications, J. Rare Earths 40 (2022) 1343–1359, https://doi.org/10.1016/j.jre.2022.04.015.
[8] H.S. Naher, B.A.H. Al-Turaihi, S.H. Mohammed, S.M. Naser, M.A. Albark, H. A. Madlool, H.A.M. Al- Marzoog, A.T. Jalil, Upconversion nanoparticles (UCNPs): synthesis methods, imaging and cancer therapy, J. Drug Deliv. Sci. Technol. 80 (2023) 104175, https://doi.org/10.1016/j.jddst.2023.104175.
[9] W. Yao, Q. Tian, W. Wu, Tunable emissions of upconversion fluorescence for security applications, Adv. Opt. Mater. 7 (2019) 1–19, https://doi.org/10.1002/adom.201801171.
[10] B. Hampel, K. Hernadi, Z. Pap, Rare earth doped luminescent materials as photocatalysts for enhanced photocatalytic reactions, in: S. Garg, A. Chandra (Eds.), Green Photocatalytic Semiconductors for Green Chemistry and Sustainable Technology, Springer, Cham, 2022, https://doi.org/10.1007/978-3-030-77371-7_9.
[11] R. Naccache, E.M. Rodríguez, N. Bogdan, F. Sanz-Rodríguez, M. del CI de la Cruz, Á.J. de la Fuente, F. Vetrone, D. Jaque, J.G. Solé, J.A. Capobianco, High resolution fluorescence imaging of cancers using lanthanide ion-doped upconverting nanocrystals, Cancers 4 (2012) 1067–1105, https://doi.org/10.3390/cancers4041067.
[12] R. Ali, S.M. Saleh, R.J. Meier, H.A. Azab, I.I. Abdelgawad, O.S. Wolfbeis, Upconverting nanoparticle based optical sensor for carbon dioxide, Sens. Actuators B Chem. 150 (2010) 126–131, https://doi.org/10.1016/j.snb.2010.07.031.
[13] H.S. Mader, O.S. Wolfbeis, Optical ammonia sensor based on upconverting luminescent nanoparticles, Anal. Chem. 82 (2010) 5002–5004, https://doi.org/10.1021/ac1007283.
[14] L. Xie, Y. Qin, H.-Y. Chen, Polymeric optodes based on upconverting nanorods for fluorescence measurements of Pb^{2+} in complex samples, Sens. Actuators B Chem. 84 (2012) 1969–1974, https://doi.org/10.1016/j.snb.2013.10.090.
[15] S.M. Saleh, F.M. Alminderej, R. Ali, O.I. Abdallah, Optical sensor film for metribuzin pesticide detection, Spectrochim. Acta - A Mol. Biomol. Spectrosc. 229 (2020) 117971, https://doi.org/10.1016/j.saa.2019.117971.
[16] S. Hao, Y. Shang, D. Li, H. Ågren, C. Yang, G. Chen, Enhancing dye-sensitized solar cell efficiency through broadband near-infrared upconverting nanoparticles, Nanoscale 9 (2017) 6711–6715, https://doi.org/10.1039/c7nr01008g.
[17] J. Zhang, H. Shen, W. Guo, S. Wang, C. Zhu, F. Xue, J. Hou, H. Su, Z. Yuan, An upconversion $NaYF_4$:Yb^{3+},Er^{3+}/TiO_2 core-shell nanoparticle photoelectrode for improved efficiencies of dye-sensitized solar cells, J. Power Sources. 226 (2013) 47–53, https://doi.org/10.1016/j.jpowsour.2012.10.073.
[18] E.D. Martínez, C.D.S. Brites, L.D. Carlos, A.F. García-Flores, R.R. Urbano, C. Rettori, Electrochromic switch devices mixing small- and large-sized upconverting nanocrystals, Adv. Funct. Mater. 29 (2019) 1–12, https://doi.org/10.1002/adfm.201807758.
[19] E.D. Martínez, C.D.S. Brites, L.D. Carlos, R.R. Urbano, C. Rettori, Upconversion nanocomposite materials with designed thermal response for optoelectronic devices, Front. Chem. 7 (2019), https://doi.org/10.3389/fchem.2019.00083.
[20] S. Sivakumar, F.C.J.M. Van Veggel, M. Raudsepp, Bright white light through up-conversion of a single NIR source from sol-gel-derived thin film made with Ln^{3+}-doped LaF_3 nanoparticles, J. Am. Chem. Soc. 127 (2005) 12464–12465, https://doi.org/10.1021/ja052583o.
[21] J. Park, K. Kim, E.J. Jo, W. Kim, H. Kim, R. Lee, J.Y. Lee, J.Y. Jo, M.G. Kim, G. Y. Jung, Plasmon enhanced up-conversion nanoparticles in perovskite solar cells for effective utilization of near infrared light, Nanoscale 11 (2019) 22813–22819, https://doi.org/10.1039/c9nr08432k.
[22] F. Trabelsi, F. Mercier, E. Blanquet, A. Crisci, R. Salhi, Synthesis of upconversion TiO_2:Er^{3+}-Yb^{3+} nanoparticles and deposition of thin films by spin coating technique, Ceram. Int. 46 (2020) 28183–28192, https://doi.org/10.1016/j.ceramint.2020.07.317.
[23] M. Fernanda Torresan, J. Morrone, C. Sorbello, R. Etchenique, P.C. Angelomé, A. Wolosiuk, Emissive platforms employing $NaYF_4$-based upconverting nanoparticles and mesoporous metal oxide thin films, Eur. J. Inorg. Chem. 2021 (2021) 2343–2352, https://doi.org/10.1002/ejic.202100177.
[24] V. Sudarsan, S. Sivakumar, F.C.J.M. Van Veggel, M. Raudsepp, General and convenient method for making highly luminescent sol-gel derived silica and alumina films by using LaF_3 nanoparticles doped with lanthanide ions (Er^{3+}, Nd^{3+}, and Ho^{3+}), Chem. Mater. 17 (2005) 4736–4742, https://doi.org/10.1021/cm051065+.
[25] E. Albert, P.A. Albouy, A. Ayral, P. Basa, G. Csík, N. Nagy, S. Roualdès, V. Rouessac, G. Sáfrán, Á. Suhajda, Z. Zolnai, Z. Hórvölgyi, Antibacterial properties of Ag–TiO_2 composite sol–gel coatings, RSC Adv. 5 (2015) 59070–59081, https://doi.org/10.1039/C5RA05990A.
[26] B. Tegze, E. Albert, B. Fodor, G. Sáfrán, Z. Hórvölgyi, Photoinduced processes of adsorbed and associated dye molecules in mesoporous titania coatings, Dye. Pigm. 167 (2019) 109–119, https://doi.org/10.1016/j.dyepig.2019.04.017.
[27] D.C. Baldini, E.H. de Faria, K.J. Ciuffi, L.A. Rocha, E.J. Nassar, TiO_2 films obtained by the sol–gel process and doped with Yb^{3+} and Er^{3+} ions, J. Sol-Gel Sci. Technol. 97 (2021) 548–555, https://doi.org/10.1007/s10971-020-05465-y.
[28] F. Trabelsi, F. Mercier, E. Blanquet, A. Crisci, R. Boichot, D. Chen, R. Salhi, Green upconversion improvement of TiO_2 codoped Er^{3+}-Yb^{3+} nanoparticles based thin film by adding ALD-Al_2O_3 for silicon solar cell applications, J. Lumin. 252 (2022), https://doi.org/10.1016/j.jlumin.2022.119282.
[29] C. Lin, M.T. Berry, R. Anderson, S. Smith, P.S. May, Highly luminescent NIR-to-visible upconversion thin films and monoliths requiring no high-temperature treatment, Chem. Mater. 21 (2009) 3406–3413, https://doi.org/10.1021/cm901094m.
[30] E.M. Rodrigues, D.A. Gálico, I.O. Mazali, F.A. Sigoli, Self-supported films of poly (methyl methacrylate) (PMMA) containing Tm III -doped upconverting core@shell nanoparticles as high sensitivity temperature optical probe, Sens. Actuators A Phys. 291 (2019) 1–6, https://doi.org/10.1016/j.sna.2019.03.019.
[31] W. Huang, C. Lu, C. Jiang, W. Wang, J. Song, Y. Ni, Z. Xu, Controlled synthesis of $NaYF_4$ nanoparticles and upconversion properties of $NaYF_4$: Yb, Er (Tm)/FC transparent nanocomposite thin films, J. Colloid Interface Sci. 376 (2012) 34–39, https://doi.org/10.1016/j.jcis.2012.02.047.
[32] N. Lyu, Y. Cao, J. Zhang, L. Zheng, B. Poudel, J.A. Piper, Y. Wang, Y. Lu, Embedding upconversion nanoparticles in polymer films toward mono-dispersity at high loading factor, Macromol. Mater. Eng. 310 (2025) 1–9, https://doi.org/10.1002/mame.202500155.
[33] W. Li, M. Xu, C. Ma, Y. Liu, J. Zhou, Z. Chen, Y. Wang, H. Yu, J. Li, S. Liu, Tunable upconverted circularly polarized luminescence in cellulose nanocrystal based chiral photonic films, ACS Appl. Mater. Interfaces 11 (2019) 23512–23519, https://doi.org/10.1021/acsami.9b05941.
[34] D.E. Achatz, R.J. Meier, L.H. Fischer, O.S. Wolfbeis, Luminescent sensing of oxygen using a quenchable probe and upconverting nanoparticles, Angew. Chemie - Int. Ed. 50 (2011) 260–263, https://doi.org/10.1002/anie.201004902.
[35] W. Wu, L. Wang, J. Yuan, Z. Zhang, X. Zhang, S. Dong, J. Hao, Formation and degradation tracking of a composite hydrogel based on UCNPs@PDA, Macromolecules 53 (2020) 2430–2440, https://doi.org/10.1021/acs.macromol.0c00072.

[36] Z. Sebestyén, E. Jakab, A. Domán, P. Bokrossy, I. Bertóti, J. Madarász, K. László, Thermal degradation of crab shell biomass, a nitrogen-containing carbon precursor, J. Therm. Anal. Calorim. 142 (2020) 301–308, https://doi.org/10.1007/s10973-020-09438-9.
[37] P. Márton, Ö.T. Nagy, D. Kovács, B. Szolnoki, J. Madarász, N. Nagy, G.S. Szabó, Z. Hórvölgyi, Barrier behaviour of partially N-acetylated chitosan layers in aqueous media, Int. J. Biol. Macromol. 232 (2023), https://doi.org/10.1016/j.ijbiomac.2023.123336.
[38] S. Li, S. Cui, D. Yin, Q. Zhu, Y. Ma, Z. Qian, Y. Gu, Dual antibacterial activities of a chitosan-modified upconversion photodynamic therapy system against drug-resistant bacteria in deep tissue, Nanoscale 9 (2017) 3912–3924, https://doi.org/10.1039/c6nr07188k.
[39] B. Zong, X. Li, Q. Xu, D. Wang, P. Gao, Q. Zhou, Enhanced eradication of enterococcus faecalis biofilms by quaternized chitosan-coated upconversion nanoparticles for photodynamic therapy in persistent endodontic infections, Front. Microbiol. 13 (2022) 1–14, https://doi.org/10.3389/fmicb.2022.909492.
[40] H. Van Duong, T.T.L. Chau, N.T.T. Dang, F. Vanterpool, M. Salmerón-Sánchez, E. Lizundia, H.T. Tran, L.V. Nguyen, T.D. Nguyen, Biocompatible chitosan-functionalized upconverting nanocomposites, ACS Omega. 3 (2018) 86–95, https://doi.org/10.1021/acsomega.7b01355.
[41] X. Wu, P. Ning, J. Tian, J. Lu, A dual-mode aptasensor for aflatoxin B1 determination based on photoelectrochemistry and upconversion fluorescence resonance energy transfer, Microchem. J. 209 (2025) 112756, https://doi.org/10.1016/j.microc.2025.112756.
[42] Y. Li, X. Wang, L. Yang, X. Xie, S. Yao, T. Min, Z. Qi, Developing FRET-based UCNP@SiO_2-AIE/AIE@DSPE-PEG2000 nanomaterials for lysosome-targeted NIR photodynamic cancer therapy, Microchim. Acta 192 (2025) 1–12, https://doi.org/10.1007/s00604-025-07584-1.
[43] S. Jayswal, M.N. Luwang, R.S. Moirangthem, Tuning the optical properties of Ln^{3+}-doped-Y_2O_3@ZnO@Au core-shell heterostructures for visible-to-NIR photon harvesting, Surf. Interfaces 44 (2024) 103775, https://doi.org/10.1016/j.surfin.2023.103775.
[44] E. Madirov, N. Hildebrandt, FRET with upconversion nanoparticles, Acc. Chem. Res. 59 (2026) 114–125, https://doi.org/10.1021/acs.accounts.5c00670.
[45] A. Das, C. Corbella Bagot, E. Rappeport, T. Ba Tis, W. Park, Quantitative modeling and experimental verification of Förster resonant energy transfer in upconversion nanoparticle biosensors, J. Appl. Phys. 130 (2021) 31–33, https://doi.org/10.1063/5.0053464.
[46] D. Lisjak, O. Plohl, J. Vidmar, B. Majaron, M. Ponikvar-Svet, Dissolution mechanism of upconverting AYF_4:Yb,Tm (A = Na or K) nanoparticles in aqueous media, Langmuir 32 (2016) 8222–8229, https://doi.org/10.1021/acs.langmuir.6b02675.
[47] B.D. Cullity, Elements of X-ray diffraction, Addison-Wesley, London, 1956.
[48] E. Hild, A. Deák, L. Naszályi, Ö. Sepsi, N. Ábrahám, Z. Hórvölgyi, Use of the optical admittance function and its WKB approximation to simulate and evaluate transmittance spectra of graded-index colloidal films, J. Opt. A Pure Appl. Opt. 9 (2007) 920–930, https://doi.org/10.1088/1464-4258/9/10/023.
[49] E. Albert, P. Basa, B. Fodor, Z. Keresztes, J. Madarász, P. Márton, D. Olasz, A. S. Rácz, G. Sáfrán, T. Szabó, B. Tegze, T. Höltzl, Z. Hórvölgyi, Experimental and computational synthesis of TiO_2 Sol-Gel coatings, Langmuir 41 (2025) 704–718, https://doi.org/10.1021/acs.langmuir.4c03959.
[50] P. Márton, B. Szolnoki, N. Nagy, A. Deák, D. Zámbó, G.S. Szabó, Z. Hórvölgyi, Wetting and swelling behaviour of N-acetylated thin chitosan coatings in aqueous media, Heliyon 10 (2024), https://doi.org/10.1016/j.heliyon.2023.e23201.
[51] P. Löbmann, Characterization of sol–gel thin films by ellipsometric porosimetry, J. Sol-Gel Sci. Technol. 84 (2017) 2–15, https://doi.org/10.1007/s10971-017-4473-1.
[52] J.S.J. Hargreaves, Some considerations related to the use of the Scherrer equation in powder X-ray diffraction as applied to heterogeneous catalysts, Catal. Struct. React. 2 (2016) 33–37, https://doi.org/10.1080/2055074X.2016.1252548.
[53] P. Márton, L. Áder, D.M. Kemény, A. Rácz, D. Kovács, N. Nagy, G.S. Szabó, Z. Hórvölgyi, Chitosan–surfactant composite nanocoatings on glass and zinc surfaces prepared from aqueous solutions, Molecules 29 (2024), https://doi.org/10.3390/molecules29133111.
[54] M. Liras, M. González-Béjar, E. Peinado, L. Francés-Soriano, J. Pérez-Prieto, I. Quijada-Garrido, O. García, Thin amphiphilic polymer-capped upconversion nanoparticles: enhanced emission and thermoresponsive properties, Chem. Mater. 26 (2014) 4014–4022, https://doi.org/10.1021/cm501663n.
[55] G. Wolansky, A. Marmur, Apparent contact angles on rough surfaces: the Wenzel equation revisited, Colloids Surf. A Physicochem. Eng. Asp. 156 (1999) 381–388, https://doi.org/10.1016/S0927-7757(99)00098-9.
[56] M.V. DaCosta, S. Doughan, Y. Han, U.J. Krull, Lanthanide upconversion nanoparticles and applications in bioassays and bioimaging: a review, Anal. Chim. Acta. 832 (2014) 1–33, https://doi.org/10.1016/j.aca.2014.04.030.
[57] V. Muhr, C. Würth, M. Kraft, M. Buchner, A.J. Baeumner, U. Resch-Genger, T. Hirsch, Particle-size-dependent förster resonance energy transfer from upconversion nanoparticles to organic dyes, Anal. Chem. 89 (2017) 4868–4874, https://doi.org/10.1021/acs.analchem.6b04662.
[58] F.M. Zehentbauer, C. Moretto, R. Stephen, T. Thevar, J.R. Gilchrist, D. Pokrajac, K. L. Richard, J. Kiefer, Fluorescence spectroscopy of Rhodamine 6G: concentration and solvent effects, Spectrochim. Acta - A Mol. Biomol. Spectrosc. 121 (2014) 147–151, https://doi.org/10.1016/j.saa.2013.10.062.